RSC Advances

PAPER

View Article Online
View Journal | View Issue

Cite this: *RSC Adv.*, 2023, **13**, 21633

Preparation of metal–organic framework combined with *Portulaca oleracea* L. extract electrostatically spun nanofiber membranes delayed release wound dressing

Yize Wang,[a] Hua Kang,[a] Jao Hu,[a] Heming Chen,[a] Huimin Zhou,[a] Ying Wang *[a] and Huizhen Ke*[b]

In this study, we prepared a polyacrylonitrile (PAN) composite nanofiber membrane comprising *Portulaca oleracea* L. extract (POE) and a zinc-based metal–organic framework (MOF) by an *in situ* growth method as a potentially new type of wound dressing with a slow drug-release effect, to solve the problem of the burst release of drugs in wound dressings. The effects of the MOF and POE doping on the nanofiber membranes were examined using scanning electron microscopy (SEM) and FTIR spectroscopy. SEM analysis revealed the dense and uniform attachment of MOF particles to the surface of the nanofiber membrane, while FTIR spectroscopy confirmed the successful fusion of MOF and POE. Furthermore, investigations into the water contact angle and swelling property demonstrated that the incorporation of the MOF and POE enhanced the hydrophilicity of the material. The results of the *in vitro* release test showed that the cumulative release rate for PAN/MOF/POE60 decreased from 66.5 ± 2.34% to 32.18 ± 1.31% in the initial 4 h and from 90.54 ± 0.79% to 65.92 ± 1.95% in 72 h compared to PAN/POE, indicating a slowing down of the drug release. In addition, the antimicrobial properties of the fiber membranes were evaluated by the disc diffusion method, and it was evident that the PAN/MOF/POE nanofibers exhibited strong inhibition against *Escherichia coli* (*E. coli*) and *Staphylococcus aureus* (*S. aureus*). The antioxidant properties of the nanofiber membranes loaded with POE were further validated through the DPPH radical scavenging test. These findings highlight the potential application of the developed nanofiber membranes in wound dressings, offering controlled and sustained drug-release capabilities.

Received 18th March 2023
Accepted 25th June 2023

DOI: 10.1039/d3ra01777j

rsc.li/rsc-advances

1 Introduction

The skin is the largest body organ and serves as a barrier against the external environment, but it is highly susceptible to damage.[1,2] While the skin possesses innate self-repair and self-healing abilities, conditions such as metabolic diseases, recurrent infections, and extensive wound areas can impede the wound-healing process, leading to increased patient discomfort and distress.[3] In this context, wound dressings play a critical role in facilitating wound healing.[4–7] An ideal wound dressing should support and protect the wound surface, absorb wound exudates, and maintain an adequate moisture balance in the wound, thus, providing a safe environment for skin regeneration and maintaining gas exchange.[8] In addition, wound dressings should be biocompatible, antimicrobial, and antioxidant.[9]

In recent years, wound dressings prepared by electrospinning have been widely used in biomedical fields. Electrospun nanofiber membranes prepared by this technique can structurally mimic the extracellular matrix of the skin and form a porous structure with a high specific surface area, which could offer high permeability and promote cell adhesion and proliferation.[10–13] Polyacrylonitrile (PAN) is a polymer with high thermal stability, spinnability, and mechanical strength, which make it an excellent material for the preparation of electrospun nanofiber membranes.[14] PAN composite nanofiber membranes loaded with curcumin, tannic acid, and silver nanoparticles were fabricated by electrospinning and showed good performance in terms of retaining excellent mechanical properties, hydrophilicity, and biocompatibility.[15]

Although various drugs or biologically active substances have been incorporated into nanofiber membranes, burst release is still a bottleneck for their application. Wound dressings that can exhibit sustained release mechanisms ensure the

[a]*College of Textile and Clothing, Xinjiang University, No. 666, Shengli Road, Tianshan, District, Urumchi 830046, China. E-mail: xjuwangying@126.com*

[b]*Fujian Engineering Research Center for Textile and Clothing, Faculty of Clothing and Design, Fujian Key Laboratory of Novel Functional Textile Fibers and Materials, Minjiang University, Fuzhou 350108, Fujian, China. E-mail: kehuizhen2013@163.com*

gradual and controlled release of drugs, thereby prolonging their therapeutic effects and reducing the frequency of drug administration.[16] Metal–organic frameworks (MOFs), composed of metal ions and organic ligands through coordination bonding, are emerging as a new material for effective wound healing.[17] In recent years, they have been widely used in gas adsorption and separation, air filtration, catalysis, and drug delivery fields due to their high specific surface area, high porosity, low skeletal density, adjustable and uniform pore size, good thermal stability, and easy functionalization.[18,19] ZIF-8 is a three-dimensional (3D) MOF with a zeolite crystal structure formed by linking zinc ions with methylimidazolate ligands, and is considered one of the best MOF materials for drug delivery due to its low biotoxicity, large porosity, antibacterial properties, and highly controlled release rate.[20,21] Research showed that ZIF-8 particles loaded with doxorubicin (DOXO) could significantly slow down release of the DOXO.[22] After 30 d, the cumulative release of DOXO was only 66%. Currently, there is a growing body of research focusing on the utilization of ZIF-8 for the controlled release of anticancer and antibiotic drugs, which has yielded promising outcomes. However, the investigation of ZIF-8 loaded with natural extracts remains relatively limited in the existing studies.

Natural extracts have gained significant attention in recent years owing to their superior biocompatibility and their potential to facilitate the process of wound healing.[23,24] *Portulaca oleracea* L. (PO) is an annual herb of the Portulacaceae family that originated in India and later spread worldwide. Several studies have found that PO is rich in biologically active ingredients, such as polysaccharides, alkaloids, polyphenols, and flavonoids.[25,26] Among these, PO flavonoids facilitate wound healing with their anti-inflammatory, antibacterial, and antioxidant properties.[27] Rashed *et al.*[28] found that PO extract (POE) could increase the amount of collagen at a wound site and promote wound healing.

In the present study, the MOF was fabricated on nanofiber membranes by an *in situ* synthesis for controlled drug release. Moreover, POE was employed as a bioactive component and incorporated into the MOF to enhance the functionality of the nanofiber membranes. The composite nanofiber membranes were subjected to various analyses, including for their surface morphology, hydrophilicity, mechanical properties, drug-release properties, antioxidant properties, and antibacterial properties.

2 Materials and methods

2.1 Materials

PO was purchased from Xinjiang Jikang Big Pharmacy Pharmaceutical Chain Co., Ltd. (China). Ethanol, petroleum ether, sodium hydroxide (NaOH), sodium chloride (NaCl), nano zinc oxide (ZnO), *N*,*N*-dimethylformamide (DMF), beef extract, PAN (M_w = 150 000), zinc acetate dehydrate ($Zn(OAc)_2 \cdot 2H_2O$), 2-methylimidazole (2-MIM), peptone, and agar were obtained from China Shanghai Aladdin Reagent Co., Ltd. 2,2-Diphenyl-1-picrylhydrazyl (DPPH) was purchased from Beijing Baioubowei Biotechnology Co., Ltd. *Escherichia coli* (*E. coli*, ATCC 25922) and *Staphylococcus aureus* (*S. aureus*, ATCC 25923) were purchased from China Nantong Kaiheng Biotechnology Co., Ltd.

2.2 Preparation of the PO extracts

The clean and dried PO was pulverized and then sieved through a 40-mesh sieve. The powder was dispersed in 70% ethanol (50 g L^{-1}) and ultrasonicated for 30 min, followed by incubation in a water bath at 60 °C for 12 h. We repeated this step three times. Subsequently, the supernatant was combined and subjected to filtration using a Brinell funnel. The resulting solution was concentrated to a volume of 50 mL using a rotary vacuum evaporator (RE-52A, Shanghai Yarong Instruments Co., Ltd., China), followed by extraction using 50 mL of petroleum ether. The lower layer was then evaporated and concentrated to yield the POE. The procedure of extraction is displayed in Fig. 1. Finally, the concentration of flavonoids in the POE was determined using the $AlCl_3$ method.

2.3 Preparation of the nanofiber membranes

PAN was dissolved in DMF to obtain a concentration of 12% (w/v) and stirred at room temperature. Later, ZnO particles were added to the PAN solution at a concentration of 2% (w/w) and continuously stirred for 12 h. The mixture was subjected to ultrasonic treatment at room temperature for 30 min to achieve a uniform blend. The resulting solution was then loaded into a standard syringe with a 5 mL capacity, equipped with a 21G blunt stainless steel needle, for the purpose of electrospinning. The electrospinning process was performed using the following parameters: a distance of 15 cm between the needle and collector, a spinning voltage of 18 kV, and a flow rate of 0.5 mL h^{-1}.

The PAN/ZnO nanofiber membranes were immersed in a $Zn(OAc)_2$/2-MIM solution and sealed at 30 °C, 60 °C, and 90 °C, respectively. After 16 h, the nanofiber membranes were thoroughly rinsed with deionized water to remove any ZIF-8 that had not adhered to the surface of the nanofibers. Subsequently, the resulting mixture was dried at 60 °C for a duration of 3 h to obtain the PAN/MOF30, PAN/MOF60, and PAN/MOF90 nanofiber membranes through an *in situ* formation process. The PAN/MOF nanofiber membranes were then immersed in the POE solution with the concentration of 10 mg mL^{-1} at 30 °C, 60 °C, and 90 °C for 12 h to obtain the PAN/MOF/POE30, PAN/MOF/POE60, and PAN/MOF/POE90 nanofiber membranes, respectively.

Moreover, nanofiber membranes of PAN with a concentration of 12% and PAN/POE with a concentration of 12% and 10% (w/v) in DMF were used as the control groups while keeping the electrospinning conditions the same. The dried nanofiber membranes were stored in drying cabinets and subsequently utilized for the characterizations, antioxidant assays, and antibacterial assays.

2.4 Scanning electron microscope (SEM) analysis

The surface micromorphology of the samples was observed using a field emission scanning electron microscopy system (SEM, su8010, Hitachi, Japan) at an accelerating voltage of 15.0

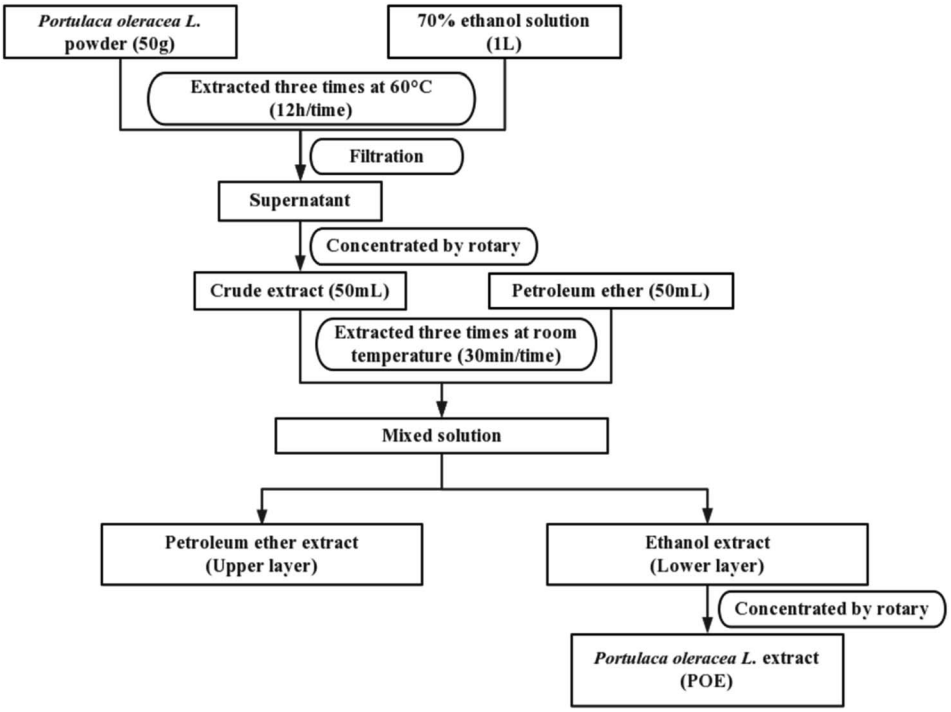

Fig. 1 Preparation of the POE.

kV. Here, 50 fibers were randomly selected from each sample and measured by ImageJ software (National Institute of Health, US). The mean diameter and frequency distribution were calculated.

2.5 Fourier transform infrared spectroscopy (FTIR) analysis

The FTIR spectrometer ATR method was employed to identify the distinctive peaks associated with the functional groups present in the composite nanofiber membranes. The spectral range analyzed was 500–4000 cm^{-1}, utilizing a resolution of 4 cm^{-1}.

2.6 Mechanical properties tests

The mechanical properties of the nanofiber membranes, such as tensile strength, breaking strength, and Young's modulus, were evaluated using a fiber tensile testing machine (YG(B) 026P, Darong Textile Instrument Co., Ltd, China). The nanofiber membranes were cut into rectangular pieces (30 × 5 mm) and fixed in the jaws of the machine. The tests were performed at a tensile rate of 10 mm min^{-1} for 20 times for each group, and the data were recorded.

2.7 Water contact angle and swelling properties

The surface properties of the nanofibers were evaluated using a water contact angle instrument (DCAT 21, DataPhysics Instruments GmbH, Germany). The nanofiber membranes (20 × 20 mm) were placed on a sample table, and 5 μL of distilled water was deposited on the surface of the nanofiber membranes. The dynamic water contact angle of the nanofiber membrane was recorded at 5, 10, and 15 s, respectively.

To evaluate the water uptake capacity of the nanofiber membranes, the weight (W_d) of the dried nanofiber membranes (20 × 20 mm) was measured. The samples were then immersed in 5 mL phosphate buffered saline solution (PBS) for 4 h at 37 °C and weighed as W_s. The water uptake (W_a) was calculated using the following eqn (1):

$$W_a = \frac{(W_s - W_d)}{W_d} \times 100\% \quad (1)$$

2.8 Drug-release studies

2.8.1 Drug-loading rate. The drug-loading capacity of the nanofibers was determined by an extraction method. The nanofiber membrane (10 mg per sample) was dissolved in 5 mL DMF, to which 10 mL PBS solution was added. The solution was subjected to ultrasonication for a duration of 30 min. Following centrifugation at 5000 rpm, the supernatant was collected at various time intervals, and the absorbance of the solution was determined at 510 nm using a UV spectrophotometer. When the absorbance values were constant, the drug-loading capacity (DL) was calculated by the following eqn (2):

$$DL = \frac{m}{M} \times 100\% \quad (2)$$

where m is the content of POE actually loaded into the nanofiber membrane, and M is the content of the initial addition of POE to the nanofiber membrane.

2.8.2 Drug-release properties. Investigations of the release of POE from the nanofiber membranes were conducted by drug-release studies. Each group was subjected to immersion in

separate vials filled with PBS solution (pH 7.4), with a sample weight of 20 mg. Subsequently, the vials were placed in a shaker set at an agitation speed of 100 rpm and maintained at a temperature of 37 °C for a duration of 72 h. At predetermined intervals, 1 mL of solution was removed and replaced with 1 mL of fresh PBS to keep the volume constant. The amount of POE released from the nanofibers was calculated based on the absorbance of the solution measured at 510 nm.

2.8.3 Kinetics of drug release. The commonly employed models, namely the zero-level eqn (3) and first-level eqn (4) models, were used for analyzing the release kinetics, along with the Higuchi model eqn (5) to describe the drug release from an insoluble matrix, and the Korsmeyer–Peppas eqn (6) model for analyzing the drug release from porous materials. All four models were used in this study to characterize the drug-release kinetics.

$$\text{Zero-level: } Q_t = Q_0 + K_0 t \tag{3}$$

$$\text{First-level: } Q_t = Q_0 e^{K_1 e t} \tag{4}$$

where Q_t is the drug-release amount in time t, Q_0 is the initial amount of the drug in solution, and K_0 and K_1 are the constants of the zero-level and the first-level model.

$$\text{Higuchi}: Q_t = K_H t^{\frac{1}{2}} \tag{5}$$

where Q_t is the drug release amount in time t, and K_H is the release-rate constant of the Higuchi model.

$$\text{Korsmeyer} - \text{Peppas}: \frac{M_t}{M_\infty} = K_k t^n \tag{6}$$

where $\frac{M_t}{M_\infty}$ is the cumulative amount of drug released at time t, K_k is the kinetic constant, and n is the diffusion coefficient. A range of diffusion coefficients was used to determine the release mode. When $n \leq 0.5$, the release mechanism is consistent with the Fick dispersion mechanism. When $0.5 < n < 1$, it is a diffusion mode in which diffusion and skeletal dissolution coexist, and when $n \geq 1$, it is a diffusion dominated by skeletal dissolution.

2.9 Antioxidant performance

The antioxidant activity of the nanofibers was determined using the DPPH scavenging method, for which DPPH ethanol solution (0.04 mg mL^{-1}) was prepared and stored in a dark place. Nanofiber membranes (50 mg per sample) were cut into pieces and immersed in 4 mL ethanol. After a period of 5 h, 2 mL of the supernatant was mixed with 2 mL of the DPPH solution, and the resulting mixture was left to react in the dark for a duration of 30 min. The absorbance of the solution was then measured at 510 nm using a UV spectrophotometer. The free-radical-scavenging rate (K%) was calculated using eqn (7):

$$K\% = \left[1 - \frac{A_i - A_j}{A_c}\right] \times 100\% \tag{7}$$

where A_i is the absorbance of the sample at 510 nm, A_j is the absorbance of the DPPH solution without the sample, and A_c is the absorbance of the control at 510 nm.

2.10 *In vitro* antibacterial activity

The antibacterial performance of the nanofiber membranes was evaluated using the disk diffusion method against *S. aureus* and *E. coli*. The nanofiber membranes were cut into circles with 8 mm diameter and kept under UV light for 30 min to disinfect both sides of the membrane. Subsequently, the nanofiber membranes were positioned onto dishes coated with *S. aureus* and *E. coli*, and the dishes were then incubated at 37 °C for a period of 24 h. The diameter of the inhibition zone was observed and documented. The experiment was conducted in triplicate.

2.10.1 Statistical analysis. All data are expressed as the mean ± SD. One-way ANOVA was used to determine the statistical significance, and the data and images were processed using Origin 2021 software.

3 Results and discussion

3.1 Determination of the flavonoid content in the POE

POE encompasses a diverse range of bioactive constituents, including a notable concentration of flavonoids, which exhibit antibacterial and antioxidant properties. Consequently, we employed the $AlCl_3$ method to assess the flavonoid content within the POE. The resulting rutin standard line is displayed in Fig. 2 ($R^2 > 0.995$), enabling the determination of the flavonoid content in POE as 43.16 mg g^{-1}, as per the rutin calibration curve.

3.2 Morphology and diameter distribution of the nanofibers

SEM was used to characterize the morphologies of the nanofiber membranes. The PAN/POE nanofibers were smooth, continuous, and bead-free (Fig. 3a and b). The average diameters of the nanofibers were 144.7 ± 27.2 nm and 159.28 ± 27.92 nm, respectively. The incorporation of POE resulted in a marginal enlargement of the nanofiber diameter, which could be attributed to the influence of POE on the solution's viscosity. SEM images of the PAN/MOF and PAN/MOF/POE samples revealed the presence of MOF particles, with an observable augmentation in the quantity of MOF particles corresponding

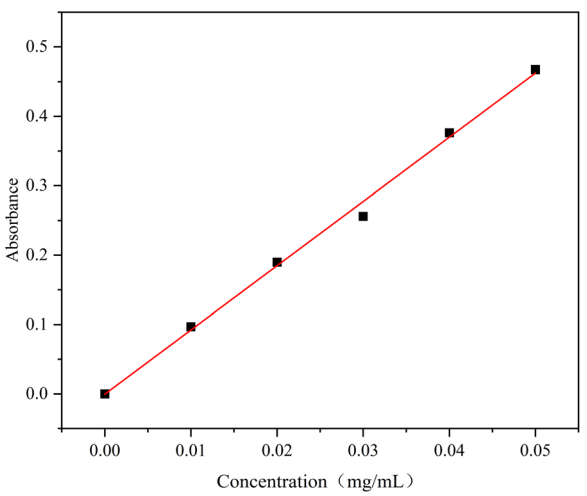

Fig. 2 Rutin calibration curve.

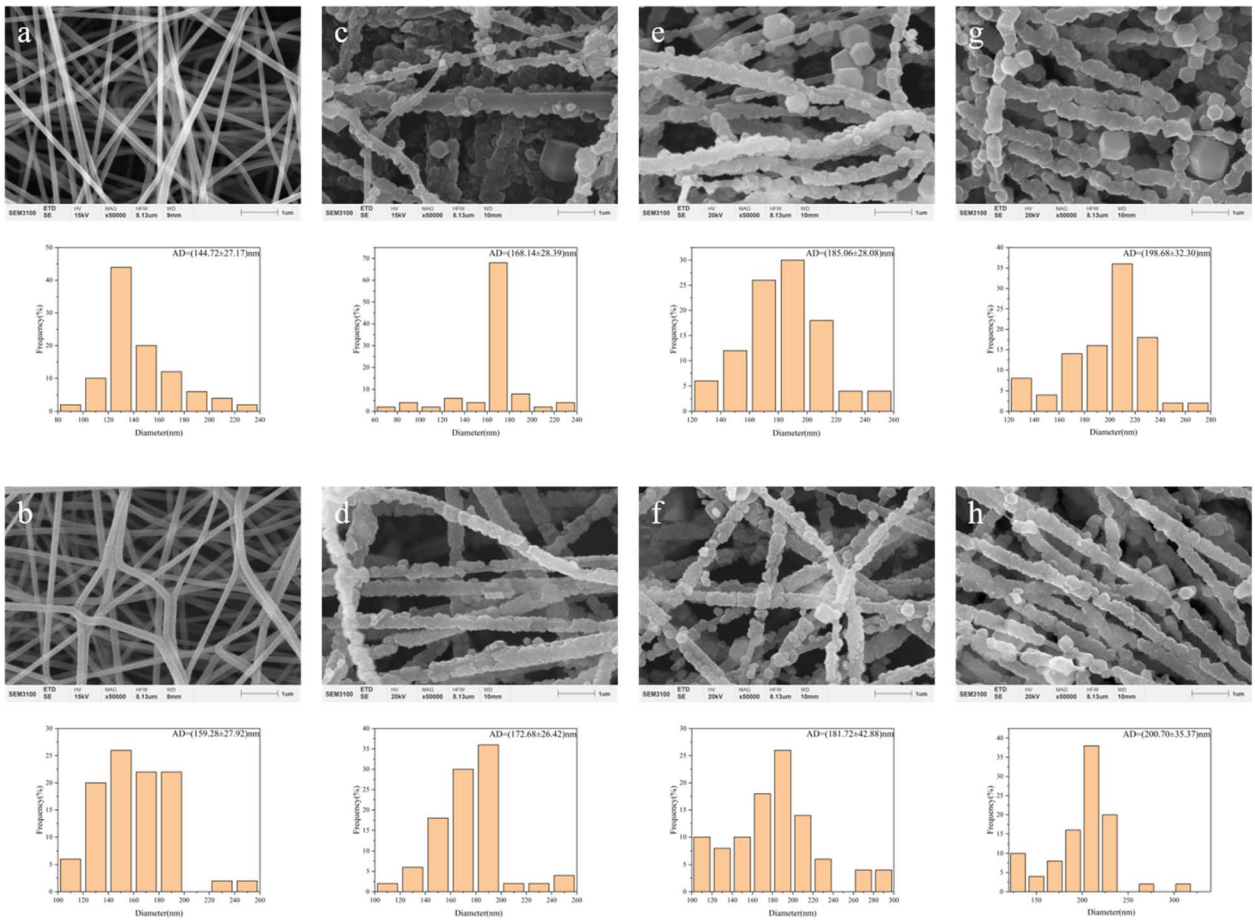

Fig. 3 SEM images and average diameters of the nanofibers: (a) PAN; (b) PAN/POE; (c) PAN/MOF30; (d) PAN/MOF/POE30; (e) PAN/MOF60; (f) PAN/MOF/POE60; (g) PAN/MOF90; (h) PAN/MOF/POE90.

to the *in situ* synthesis temperature. At 90 °C, the MOF particles were coated homogeneously on the nanofibers. The diameter of the PAN/MOF90 and PAN/MOF/POE90 were 198.68 ± 32.30 nm and 200.70 ± 35.37 nm, respectively. The diameters of the nanofiber membranes were not influenced by adding the POE.

3.3 FTIR analysis

The presence of POE and MOF in the nanofiber membranes was investigated *via* FTIR spectroscopy, as shown in Fig. 4. The peaks at 2242 and 1730 cm^{-1} were assigned to the C≡N and C═O bond stretching vibrations in PAN.[29] The presence of flavonoids in POE was indicated by a broad peak at 3338 cm^{-1}, corresponding to the stretching vibrations of –OH, as well as a sharp peak at 829 cm^{-1}, associated with the ═C–H stretching vibrations of the flavonoids.[30] Further, the band at 2940 cm^{-1} corresponded to the –C–H–stretching vibrations of the ZIF-8 ring aromatics.[31] These results indicated the presence of POE and MOF in the nanofiber membranes.

3.4 Water contact angle and swelling properties

Hydrophilic nanofiber membranes facilitate cell adhesion, diffusion, and proliferation, which promotes wound healing.[32] Therefore, the hydrophilicity of the material was evaluated based on the dynamic contact angle of water. In general, a contact angle in the range of 0°–90° indicates a good hydrophilicity of a material, while a contact angle in the range of 90°–180° indicates a good hydrophobicity of a biological

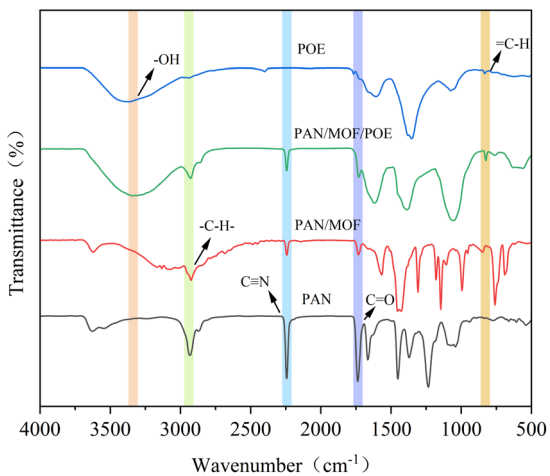

Fig. 4 FTIR spectra of the nanofiber membranes.

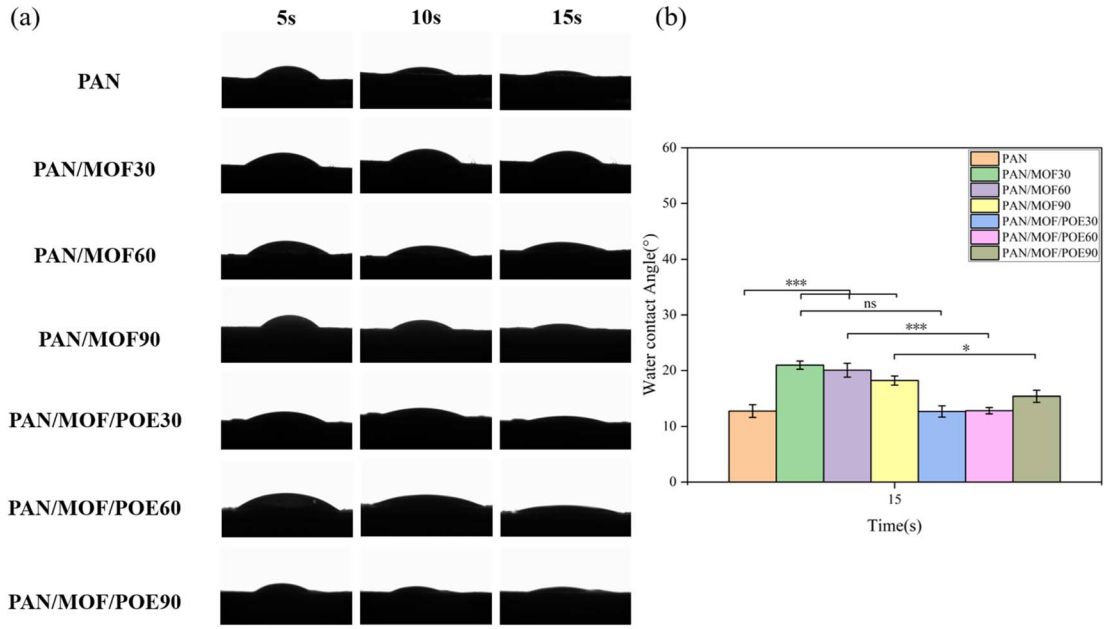

Fig. 5 Hydrophilic analysis of the nanofiber membranes: (a) variation of water droplets on individual membranes with the contact time, (b) water contact angle of the nanofiber membrane at 15 s; statistical significance: $*p < 0.05$, $p < 0.001$.

material.[33,34] The results of this study are presented in Fig. 5. Due to the hydrophilic nature of PAN itself, the water contact angles of pure PAN nanofiber membranes were 33.0 ± 1.40°, 18.3 ± 1.65°, and 12.8 ± 1.14° at 5, 10, and 15 s, respectively. The MOF particles on the nanofibers improved the hydrophilic properties of the membranes. The increase in the reaction temperature *in situ* led to improved hydrophilic properties of the membranes. The contact angle of the PAN/MOF30 nanofiber membrane was measured as 21.0 ± 0.74° at 15 s, which was found to be lower compared to that of the PAN/MOF90 nanofiber membrane, which recorded a value of 18.2 ± 0.82°. This disparity could be attributed to the higher presence of micropores within the MOF structure, facilitating water absorption. The addition of the POE also improved the hydrophilicity of the PAN/MOF/POE nanofiber membranes, and the water contact angles of PAN/MOF/POE30, PAN/MOF/POE60, and PAN/MOF/POE90 were 12.7 ± 1.00°, 12.8 ± 0.57°, and 15.4 ± 1.06°, respectively, at 15 s. This may have been due to the high content of hydrophilic substances, such as flavonoids and polysaccharides, in POE.[35]

The swelling behavior is another important parameter for assessing the fluid-absorption capacity of a wound dressing. Ideally, the swelling rate of a wound dressing should be within the range of 100–900%, allowing for the absorption of exudates and the delivery of bioactive substances and nutrients through permeation.[36,37] Fig. 6 presents the swelling rate of the nanofiber membranes after immersion in PBS for a duration of 4 h. The PAN nanofiber membrane exhibited a swelling rate of 164.67 ± 20.21%. When adding the MOF structure, the swelling rate of the membranes increased from 199.67 ± 16.50% for PAN/MOF30 to 244.00 ± 22.61% for PAN/MOF90 due to the increased micropores in the PAN/MOF structures. Besides that, the addition of POE also increased the swelling rate for PAN/MOF/POE30, PAN/MOF/POE60, and PAN/MOF/POE90 with swelling rates of 365.00 ± 53.02%, 288.00 ± 25.00%, and 283.33 ± 38.19%, respectively, attributed to the large number of hydroxyl groups in the POE. The PAN/MOF/POE30 nanofiber membrane exhibited superior swelling performance compared to the other two groups. This could be attributed to the lower process temperature, which preserved a higher concentration of hydrophilic flavonoid substances. The observed swelling rate of the membrane corresponded with the findings of the water contact angle test, confirming its excellent hydrophilicity.[38]

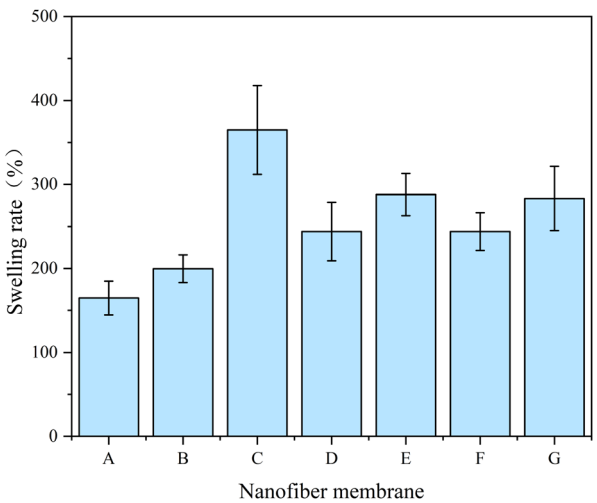

Fig. 6 Water absorption capacity of nanofibers after 4 h immersion in PBS (A), PAN (B), PAN/MOF30, (C) PAN/MOF60, (D) PAN/MOF90, (E) PAN/MOF/POE30, (F) PAN/MOF/POE60, (G) PAN/MOF/POE90.

3.5 Mechanical properties

An ideal wound dressing should also have good mechanical properties to withstand forces generated by body movement.[39] The fundamental indicators for assessing the mechanical properties of a wound dressing include its breaking strength, elongation at break, and Young's modulus. Fig. 7 exhibits the breaking strength, and elongation at break of pure PAN nanofiber membranes, which were 3.03 ± 0.47 MPa and 51.03 ± 5.15% MPa, respectively. However, with the introduction of MOF structures, the breaking strength of the PAN/MOF increased initially and then decreased. This observed phenomenon could be attributed to the elevated reaction temperature and the resulting increase in brittleness induced by the presence of inorganic MOF structures.[40] Furthermore, the addition of POE did not have a substantial impact on the breaking strength.

3.6 Drug-release studies

3.6.1 Drug-loading rate. The POE-loading capacity of the nanofiber membranes was determined using the drug-loading rate determination assay. Table 1 presents the drug-loading rates of PAN/MOF/POE30, PAN/MOF/POE60, and PAN/MOF/POE90, which were 62.48 ± 2.88%, 51.65 ± 1.17%, and 29.67 ± 2.14%, respectively. The drug-loading rate exhibited a gradual decline as the reaction temperature increased, which could be attributed to the detrimental effect of high temperatures on the integrity of the bioactive components present in the POE.[41]

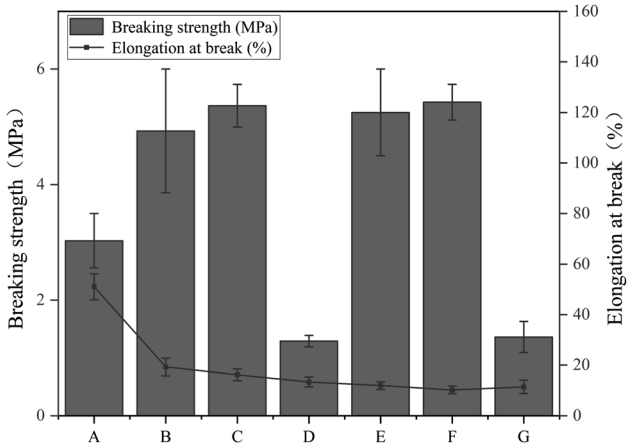

Fig. 7 Mechanical properties of each group of nanofiber membranes: (A) PAN, (B) PAN/MOF30, (C) PAN/MOF60, (D) PAN/MOF90, (E) PAN/MOF/POE30, (F) PAN/MOF/POE60, (G) PAN/MOF/POE90.

Table 1 Drug-loading rate of nanofiber membranes prepared at different temperatures

	Drug-loading rate (%)
PAN/POE	51.53 ± 1.30
PAN/MOF/POE30	62.48 ± 2.88
PAN/MOF/POE60	51.65 ± 1.17
PAN/MOF/POE90	29.67 ± 2.14

3.6.2 Drug-release properties. In the present study, MOF was used as a carrier for the POE to achieve prolonged drug release. In addition to the PAN/MOF/POE60 group, a control group PAN/POE containing an equivalent amount of POE was included for comparison. Both the PAN/POE and PAN/MOF/POE60 groups displayed an initial burst release of POE within the first 4 h, as illustrated in Fig. 8. However, the release quantity from the PAN/POE group was notably higher than that from the PAN/MOF/POE60 group ($p < 0.001$). The amounts of POE released from the PAN/POE and PAN/MOF/POE60 groups were 66.5 ± 2.34% and 32.18 ± 1.31%, respectively. After 72 h, the POE released from the PAN/POE group reached 90.54 ± 0.79%, while only 65.92 ± 1.95% was released from PAN/MOF/POE60 ($p < 0.001$, compared to PAN/POE), which might be attributed to the porous structure of the MOF, resulting in the delayed POE-release rate. The release-amount trend observed in the PAN/MOF/POE30 and PAN/MOF/POE90 groups was comparable to that of the PAN/MOF/POE60 group. However, the release amount of the PAN/MOF/POE30 group was higher than the other groups, possibly due to the highest loading rate of the PAN/MOF/POE30 group.[42]

3.6.3 Kinetics of drug release. The study also analyzed the release process of PAN/MOF/POE nanofiber membranes using mathematical kinetic models. The findings in Table 2 indicate that the release data of PAN/MOF/POE could be best fitted by the Korsmeyer–Peppas release model ($R^2 > 0.95$, ($n < 0.5$)). This observation suggests that the release mechanisms of POE in these groups were primarily governed by Fickian diffusion. The concentration difference of POE between the drug-loaded nanofiber and solution may be the underlying cause of this phenomenon. Moreover, the release mechanism could fit well with the Higuchi release model ($R^2 > 0.92$), indicating that diffusion was the primary release process.[43] In the acidic solution, the MOF skeleton would dissolve and diffuse so that the drug, which is loaded in the MOF, would diffuse rapidly. In contrast, the dissolution rate of the MOF skeleton is slower in

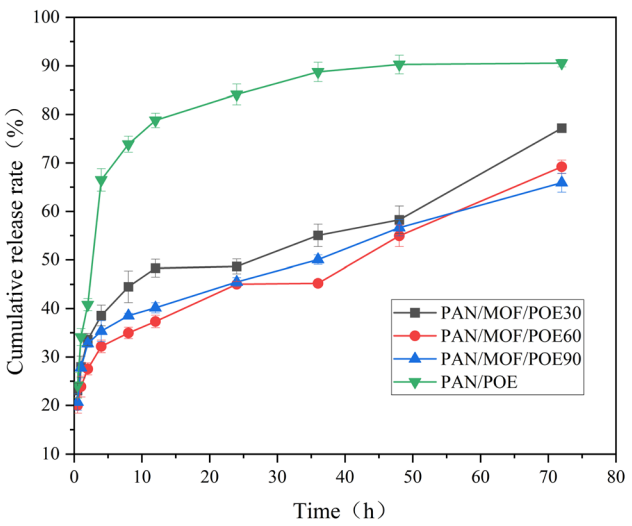

Fig. 8 Cumulative release profiles of nanofiber membranes within 72 h.

Table 2 Kinetics models of drug release from the nanofiber membranes

	Zero-order kinetic		First-order kinetic		Higuchi kinetic		Korsmeyer–Peppas kinetic		
Sample	K_0	R^2	K_1	R^2	K_H	R^2	K_k	n	R^2
PAN/MOF/POE30	0.62	0.866	0.013	0.729	5.71	0.925	1.44	0.21	0.958
PAN/MOF/POE60	0.6	0.933	0.014	0.821	5.48	0.959	1.36	0.22	0.958
PAN/MOF/POE90	0.53	0.892	0.012	0.744	4.95	0.959	1.42	0.2	0.956

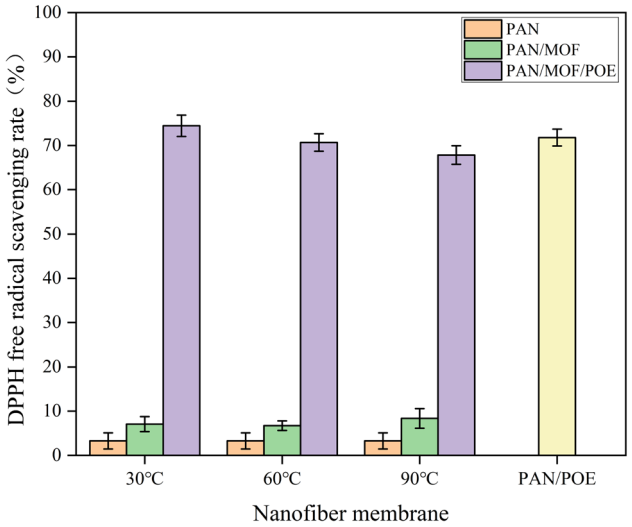

Fig. 9 Antioxidant activities of the nanofiber membranes.

a neutral solution, leading to a hindered drug release. Consequently, the release rate of POE in PAN/MOF/POE was notably slower compared to in PAN/POE in this study.[44]

3.7 Antioxidant activity

Studies have shown that excessive free radicals may lead to protein degradation in the extracellular matrix (ECM) and injury to epithelial cells, which could decelerate the healing rate.[45] Hence, in this study, the abundant flavonoids present in the POE were utilized as antioxidants. The DPPH assay, a widely adopted method for evaluating antioxidant activity, was employed to assess the antioxidant potential of the nanofiber membranes.[46] As depicted in Fig. 9, the PAN/MOF/POE nanofiber membranes exhibited robust antioxidant activity, albeit slightly lower than that of the PAN/POE group. Conversely, groups without POE exhibited considerably low antioxidant activities. The DPPH scavenging activity of PAN/MOF/POE and

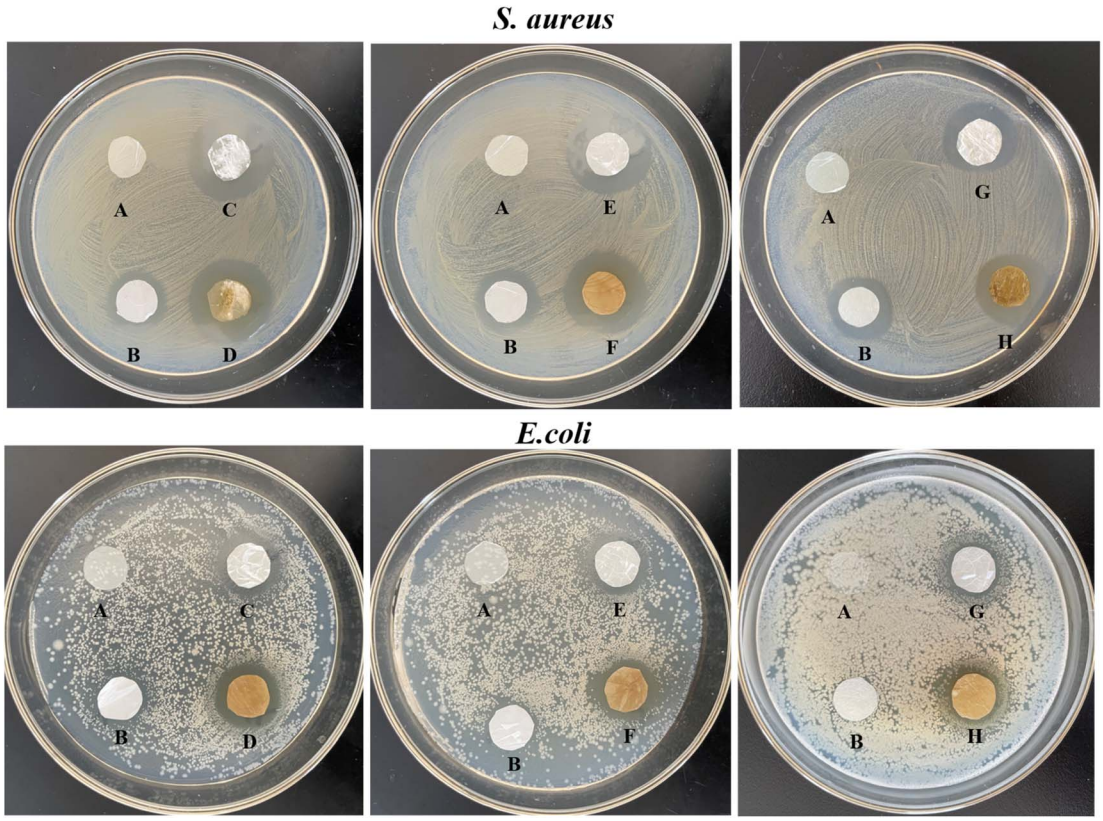

Fig. 10 Antibacterial activity of the nanofiber membranes against *S. aureus* and *E. coli*: (A) PAN, (B) PAN/POE, (C) PAN/MOF30, (D) PAN/MOF/POE30, (E) PAN/MOF60, (F) PAN/MOF/POE60, (G) PAN/MOF90, (H) PAN/MOF/POE90.

Table 3 Diameters of the inhibitory zones of the nanofiber membranes. Data are expressed as the mean ± SD ($n = 3$)

Groups	Diameters of the inhibitory zone (mm)	
	S. aureus	*E. coli*
PAN	0	0
PAN/POE	10.11 ± 0.46^a	9.21 ± 0.30^a
PAN/MOF30	19.65 ± 1.46^a	17.25 ± 1.01^a
PAN/MOF60	21.52 ± 0.71^a	16.77 ± 1.76^a
PAN/MOF90	18.91 ± 0.69^a	15.70 ± 2.29^a
PAN/MOF/POE30	21.61 ± 1.31^a	19.03 ± 1.45^a
PAN/MOF/POE60	21.70 ± 1.96^a	17.47 ± 1.06^a
PAN/MOF/POE90	19.05 ± 0.44^a	15.88 ± 1.69^a

[a] In the same column indicates significant difference $P < 0.001$ PAN/MOF and PAN/MOF/POE *vs.* PAN.

the reaction temperature showed a negative correlation, attributed to the decreased POE content with the increase in reaction temperature.

3.8 Antibacterial activity

Ideal wound dressings should possess antimicrobial properties to prevent bacterial infections and promote wound healing by reducing inflammation.[47] The antibacterial characteristics of the nanofiber membranes were assessed through the disc diffusion method, and the results are illustrated in Fig. 10 and Table 3. Pure PAN exhibited no antibacterial properties, whereas the PAN/MOF nanofiber membranes displayed a notable inhibition zone against both *S. aureus* and *E. coli*.[48–50] The mean diameters of the inhibition zone for PAN/MOF30, PAN/MOF60, and PAN/MOF90 were 19.65 ± 1.46, 21.52 ± 0.71, and 18.91 ± 0.69 mm against *S. aureus* and 17.25 ± 1.01 mm, 16.77 ± 1.76, and 15.70 ± 2.29 mm against *E. coli*, respectively. This phenomenon was possibly due to the presence of Zn^{2+} in ZIF-8, which could penetrate bacteria and disrupt the intracellular metabolic pathways.[51,52] Moreover, the addition of POE to the nanofiber membranes aimed at enhancing their antibacterial activity resulted in a slight enhancement in the average diameter of the inhibition zone observed in the PAN/MOF/POE groups. This improvement could be attributed to the presence of flavonoids in the POE, which can elevate the concentration of reactive oxygen species (ROS) within bacteria and induce DNA breakage.[53–55]

4 Conclusion

Despite the extensive research into wound dressings prepared by electrospinning in accelerating wound healing, the explosive release of drugs in electrospun membranes is still a problem that needs to be addressed. In this study, we synthesized MOF *in situ* on nanofibers at three distinct reaction temperatures, as MOF is a favorable nanocarrier for regulating drug release. Furthermore, to examine the impact of the MOF on retarding drug release, we incorporated POE, a bioactive substance known for its ability to accelerate wound healing, into the MOF to enhance the wound-healing properties. The results showed that with the addition of MOF, the cumulative drug-release rate of the PAN/MOF/POE60 nanofiber membrane, which has better physical properties, decreased from 66.5 ± 2.34% for PAN/POE to 32.18 ± 1.31% for PAN/MOF/POE60 in the first 4 h and from 90.54 ± 0.79% for PAN/POE to 65.92 ± 1.95% for PAN/MOF/POE60 in 72 h. The MOF structure reduced the drug-release rate significantly. Furthermore, the inclusion of POE imparted antibacterial and antioxidant capabilities to the nanofiber membranes, which are crucial for promoting wound healing. The nanofiber membranes developed in this study hold great potential for utilization in the realm of wound dressings with controlled release functionality.

Conflicts of interest

The authors declare that they have no conflicts of interest.

Acknowledgements

This research was supported by The General Program of Xinjiang Natural Science Foundation (2021D01C059); The Xinjiang University Scientific Research Fund of Doctor (2019720001); The Open Project Program of Fujian Key Laboratory of Novel Functional Textile Fibers and Materials, Minjiang University China (FKLTFM21XX).

References

1 J. Kim and K. W. Lee, *Curr. Pharm. Des.*, 2018, **24**, 1533–1550.
2 C. N. Vassallo and D. Wall, *BioEssays*, 2016, **38**, 306–315.
3 V. L. Madhusudhan, *Int. Wound J.*, 2015, **13**, 1129–1136.
4 C. Xian, Z. Zhang, X. You, Y. Fang and J. Wu, *Adv. Funct. Mater.*, 2022, **32**, 2202410.
5 G. Liu, Y. Zhou, Z. Xu, Z. Bao, L. Zheng and J. Wu, *Chin. Chem. Lett.*, 2023, **34**, 107705.
6 H. Zhong, J. Huang, J. Wu and J. Du, *Nano Res.*, 2022, **15**, 787–804.
7 H. Wang, Z. Xu, Q. Li and J. Wu, *Eng. Regen.*, 2021, **2**, 137–153.
8 K. Chen, F. Y. Wang, S. Y. Liu, X. F. Wu, L. M. Xu and D. K. Zhang, *Int. J. Biol. Macromol.*, 2020, **148**, 501–509.
9 P. Xin, S. Han, J. Huang, C. Zhou, J. Zhang, X. You and J. Wu, *Chin. Chem. Lett.*, 2022, **34**, 108125.
10 X. Gao, S. Han, R. Zhang, G. Liu and J. Wu, *J. Mater. Chem. B*, 2019, **7**, 7075–7089.
11 E. Masaeli, F. Karamali, S. Loghmani, M. B. Eslaminejad and M. H. Nasr-Esfahani, *J. Mater. Chem. B*, 2017, **5**, 765–776.
12 K. Souliotis, I. Kalemikeraki, M. Saridi, M. Papageorgiou and A. Kalokerinou, *Wound Repair Regen.*, 2016, **24**, 596–601.
13 N. Lin and B. Q. Zuo, *J. Biomater. Sci., Polym. Ed.*, 2021, **32**, 1983–1997.
14 S. Hashemikia, F. Farhangpazhouh, M. Parsa, M. Hasan, A. Hassanzadeh and M. Hamidi, *Int. J. Pharm.*, 2021, **597**, 120313.
15 P. H. Chen, M. Y. Chai, Z. X. Mai, M. J. Liao, X. Q. Xie, Z. W. Lu, W. Q. Zhang, H. Zhao, X. M. Dong, X. J. Fu,

F. Ko, X. T. Shi, W. X. Zheng and W. Y. Zhou, *Mater. Today Commun.*, 2022, **31**, 103336.
16 J. Li, X. Li and P. Liu, *Colloids Surf., B*, 2020, **185**, 110608.
17 Y. Liu, Y. Z. Huo, X. X. Wang, S. J. Yu, Y. J. Ai, Z. S. Chen, P. Zhang, L. Chen, G. Song, N. S. Alharbi, S. O. Rabah and X. K. Wang, *J. Cleaner Prod.*, 2020, **278**, 123216.
18 Q. Zhang, C. F. Xue, J. X. Wang, R. C. Huang, X. G. Hao and K. X. Li, *New Res. Carbon Mater.*, 2021, **36**, 322–335.
19 F. P. Kinik, A. Uzun and S. Keskin, *ChemSusChem*, 2017, **10**, 2842–2863.
20 Y. Wei, M. Chang, J. R. Liu, N. Wang and J. X. Wang, *Nanoscale*, 2022, **14**, 2793–2801.
21 M. R. Cai, L. Y. Qin, L. N. Pang, B. R. Ma, J. Bai, J. Liu, X. X. Dong, X. B. Yin and J. Ni, *New J. Chem.*, 2020, **44**, 17693–17704.
22 I. B. Vasconcelos, T. G. Silva, G. C. G. Militão, T. A. Soares, N. M. Rodrigues, M. O. Rodrigues, N. B. Costa, R. O. Freire and S. A. Junior, *RSC Adv.*, 2012, **2**, 9437–9442.
23 P. Xin, S. Han, J. Huang, X. You and J. Wu, *ACS Appl. Mater. Interfaces*, 2022, **14**, 34480–34487.
24 Y. Fang, G. Li, C. Huang, K. Huang, Y. Zhao, T. Nie and J. Wu, *Int. J. Biol. Macromol.*, 2023, **229**, 123–135.
25 M. Iranshahy, B. Javadi, M. Iranshahi, S. P. Jahanbakhsh, S. Mahyari, F. V. Hassani and G. Karimi, *J. Ethnopharmacol.*, 2017, **205**, 158–172.
26 F. Gatea, E. D. Teodor, A. M. Seciu, E. Nagodă and G. L. Radu, *Med. Chem. Res.*, 2017, **26**, 1516–1527.
27 S. H. Chang, L. P. Wang, T. Zhang, Y. Nie, R. J. Liu and L. H. Ma, *RSC Adv.*, 2020, **10**, 7321–7327.
28 A. N. Rashed, F. U. Afifi and A. M. Disi, *J. Ethnopharmacol.*, 2003, **88**, 131–136.
29 K. Ruhland, R. Frenzel, R. Horny, A. Nizamutdinova, L. Wüllen, J. Moosburger-Will and S. Horn, *Polym. Degrad. Stab.*, 2017, **146**, 298–316.
30 Y. Duan, Z. M. Ying, F. He, X. X. Ying, L. Q. Jia and G. L Yang, *Fitoterapia*, 2021, **153**, 104993.
31 S. Wang and S. Q. Zhang, *J. Inorg. Organomet. Polym. Mater.*, 2017, **27**, 1317–1322.
32 S. G. Jin, A. M. Yousaf, K. S. Kim, D. W. Kim, D. S. Kim, J. K. Kim, C. S. Yong, Y. S. Youn, J. O. Kim and H. G. Choi, *Int. J. Pharm.*, 2016, **501**, 160–166.
33 T. Brozova and M. Raudensky, *J. Elastomers Plast.*, 2018, **50**, 737–746.
34 F. Fu, D. Wang, M. Shen, S. B. Shang, Z. Q. Song and J. Song, *RSC Adv.*, 2019, **9**, 29788–29795.
35 M. Araújo, Y. Franco, M. Messias, G. Longato, J. Pamphile and P. Carvalho, *Planta Med.*, 2017, **83**, 7–22.
36 M. T. Khorasani, A. Joorabloo, A. Moghaddam, H. Shamsi and Z. MansooriMoghadam, *Int. J. Biol. Macromol.*, 2018, **114**, 1203–1215.
37 H. Adeli, M. T. Khorasani and M. Parvazinia, *Int. J. Biol. Macromol.*, 2019, **122**, 238–254.
38 Z. Q. Zhang, Q. Han, S. T. Zhang, X. Y. Guo, H. L. Huang, F. Yang and C. L. Zhong, *ACS Sustainable Chem. Eng.*, 2022, **10**, 11867–11874.
39 X. M. Zhang, H. N. Wan, W. W. Lan, F. Y. Miao, M. Qin, Y. Wei, Y. C. Hu, Z. W. Liang and D. Huang, *J. Mech. Behav. Biomed. Mater.*, 2022, **126**, 105044.
40 R. Ramalingam, C. Dhand, C. M. Leung, S. T. Ong, S. K. Annamalai, M. Kamruddin, N. K. Verma, S. Ramakrishna, R. Lakshminarayanan and K. D. Arunachalam, *Mater. Sci. Eng. Carbon*, 2019, **98**, 503–514.
41 J. C. Gouot, J. P. Smith, B. P. Holzapfel, A. R. Walker and C. Barril, *J. Exp. Bot.*, 2019, **70**, 397–423.
42 N. Hedayati, M. Montazer, M. Mahmoudirad and T. Toliyat, *Carbohydr. Polym.*, 2020, **240**, 116267.
43 W. L. Liu, H. Zhang, W. Zhang, M. Wang, J. H. Li, Y. Zhang and H. Y. Li, *J. Mater. Sci.*, 2020, **55**, 15275–15287.
44 H. W. Guo, S. j. Tan, J. Gao and L. Wang, *J. Mater. Chem. B*, 2020, **8**, 1759–1770.
45 P. L. Thi, Y. Lee, D. L. Tran, T. T. H. Thi, J. I. Kang, K. M. Park and K. D. Park, *Acta Biomater.*, 2020, **103**, 142–152.
46 M. Zamani, A. M. Delfani and M. Jabbari, *Spectrochim. Acta, Part A*, 2018, **201**, 288–299.
47 C. Fu, Z. P. Qi, C. L. Zhao, W. J. Kong, H. R. Li, W. L. Guo and X. Y. Yang, *J. Biol. Eng.*, 2021, **15**, 17.
48 S. Sun, W. C. Dai, H. S. Yu, Y. H. Wang, X. L. Wang and S. Peng, *Indian J. Anim. Res.*, 2015, **49**, 827–829.
49 X. J. Fan, S. Z. Liu, H. H. Li, J. He, J. T. Feng, X. Zhang and H. Yan, *Meat Sci.*, 2019, **147**, 82–90.
50 M. Taheri, D. Ashok, T. Sen, T. G. Enge, N. K. Verma, A. Tricoli, A. Lowe, D. R. Nisbet and T. Tsuzuki, *Chem. Eng. J.*, 2021, **413**, 127511.
51 D. Luo, C. J. Wang, Y. Tong, C. Liu, Y. M. Xiao, Z. X. Zhu, D. N. Liu and Y. Y. Wang, *RSC Adv.*, 2020, **10**, 7360–7367.
52 X. X. Wei, D. P. Xu, K. J. Ge, S. Y. Qi and Y. Chen, *J. Inorg. Organomet. Polym. Mater.*, 2020, **30**, 3862–3868.
53 Y. K. Du, J. Liu, X. M. Li, F. F. Pan, Z. G. Wen, T. C. Zhang and P. L. Yang, *Int. J. Food Prop.*, 2017, **20**, 534–542.
54 M. M. Kasprzak, A. Erxleben and J. Ochocki, *RSC Adv.*, 2015, **5**, 45853–45877.
55 T. T. Yang, D. H. Wang and X. Y. Liu, *J. Mater. Chem. B*, 2020, **8**, 406–415.